FERMILAB-CONF-13-191-APC

TRANSVERSE-TO-LONGITUDINAL EMITTANCE EXCHANGE AT THE FERMILAB ADVANCED SUPERCONDUCTING TEST ACCELERATOR

C.R. Prokop [1], P. Piot [1,2], B.E. Carlsten [3], M. Church[2]
[1] Department of Physics, Northern Illinois University DeKalb, IL 60115, USA
[2] Fermi National Accelerator Laboratory, Batavia, IL 60510, USA
[3] Los Alamos National Laboratory, Los Alamos, NM, 87544 USA

A variable-dispersion bunch compressor chicane with a transverse-deflecting cavity (TDC) may serve as a transverse-to-longitudinal emittance exchangers (EEX). In this paper, we present a design and simulations of a chicane-based EEX for eventual implementation at Fermilab's Advanced Superconducting Test Accelerator (ASTA). Such a beamline is foreseen to enable bunch current profile shaping, bunch compression, and emittance repartioning to tailor the beam per user's requirements.

I. INTRODUCTION

The usability of electron beams in linear accelerators is often limited by the longitudinal and/or transverse emittances and phase space distributions. Collective effects during the bunch generation, transport, and acceleration generally increase the emittance. Conventional beamlines can mitigate this emittance growth but generally not reduce or repartition the emittances.

Transverse-to-longitudinal emittance exchangers allow for the repartitioning and shaping of the beam's phase space. A simple emittance exchanger beamline (EEX) consisting of a transverse-deflecting cavity (TDC) flanked by two doglegs was proposed [1] and experimentally demonstrated at Fermilab's A0 photoinjector [2, 3]. This configuration displaces the beam from its original direction which may significantly impact the design of a given accelerator. At the Advanced Superconducting Test Accelerator (ASTA) currently in construction at Fermilab [4], the use of such an exchanger would require the downstream superconducting linac to be off-axis from the main linac which in turn would significantly reduce the flexibility of ASTA (experiments not requiring emittance exchange would still have to go through a double dogleg system and chromatic correction would have to be implemented). In this paper, we explore an alternative emittance-exchanger design, which does not offset the beam direction. We also discuss plans for a double emittance exchanger [5]. Lastly, we explore the design and performance of the EEX in the context of actual experimental parameters, for which we are guided with the studies performed in Ref. [7] using the codes ELEGANT [8] and IMPACT-Z [9].

In this paper, we represent the phase space coordinates of an electron as $\widetilde{\mathbf{U}} \equiv (x, x,', y, y', z, \delta)$ where x, y, and z are respectively the horizontal, vertical and longitudinal positions and x' and y' are the transverse divergences. The quantity δ is the fractional longitudinal momentum spread. We correspondingly define ε_u $(u = x, y, z)$ to be the normalized emittances associated to each degree of freedom. We consider phase-space exchanges between only the horizontal and longitudinal dimension and define the four-dimensional position $\widetilde{\mathbf{X}} \equiv (x, x', z, \delta)$ which is, to first order, transformed by a 4×4 transport matrix R.

Considering an EEX beamline composed of a TDC located between two dispersive sections, several conditions must be satisfied [10] to insure the EEX transfer matrix is 2×2-block antidiagonal. The TDC normalized strength [11] [$\kappa \equiv \frac{2\pi}{\lambda}\frac{eV_x}{pc}$, where e, c, p, V_x and λ are respectively the electronic charge, speed of light, beam momentum, integrated deflecting voltage, and the wavelength of the deflecting mode] has to satisfy $\kappa = -1/\eta_x$ where η_x is the value at the TDC location (i.e. generated by the upstream dispersive section). Given $\eta_x\prime$, the dispersion derivative w.r.t. the longitudinal coordinate at the TDC, the downstream dispersive section must satisfy the equations

$$R_{16} = \eta_x R_{11} + R_{12}\eta_x\prime \quad (1)$$

$$R_{26} = \eta_x R_{21} + R_{22}\eta_x\prime \quad (2)$$

where R_{ij} are elements of the transfer matrix of the downstream beamline. The solutions considered in this paper consists of an upstream beamline arrange as a dogleg with $\eta_x\prime = 0$. The downstream beamline consists of a flipped dogleg of equal lengths and bending angles as the upstream dogleg. This configuration does not alter the beam's direction. Equations 1 assume a thin-lens treatment of the TDC. The thick-lens transfer matrix contains a non-vanishing R_{65} element which leads to spurious coupling. As proposed in Ref. [5] this term can be cancelled using an accelerating mode cavity operated at zero-crossing and located downstream of the TDC.

To quantify the emittance-exchange process we introduce the figure of merits $\mathcal{F}_{zx} \equiv \frac{\varepsilon_{zf}}{\varepsilon_{xi}}$ and $\mathcal{F}_{xz} \equiv \frac{\varepsilon_{xf}}{\varepsilon_{zi}}$ to describe the ratio of the final to the initial emittances for the two exchanged planes. Ideal emittance exchange corresponds to $\mathcal{F} = 1$. Many sources reduce the quality of the exchange, including (1) second-order effects that arise from the finite beam size and energy spread and (2) collective effects such as space charge (SC) and coherent synchrotron radiation (CSR). Each of these sources of degradation need to be addressed and controlled as discussed below.

Operated by Fermi Research Alliance, LLC under Contract No. De-AC02-07CH11359 with the United States Department of Energy.

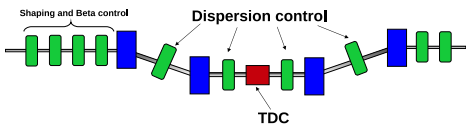

FIG. 1: Emittance-exchanger design used for this study. Quadrupole magnets inside the chicane control the dispersion for the emittance exchange, while the upstream/downstream telescopes control longitudinal/transverse output.

II. CHICANE EEX WITH NOMINAL DISPERSION

The chicane-style EEX (CX) contains quadrupole magnets placed in the dispersive region control the dispersion η_x and its derivative η_x' along the beamline, while satisfying the core requirements for perfect exchange. We first explore on the case where the quadrupoles are used only to change the *sign* of the dispersion of the first dogleg while keeping the second dogleg at its geometric value. We refer to this configuration as the nominal-dispersion EEX (NDCX). The upstream and downstream quadrupoles shape the final longitudinal and transverse distributions, respectively. The dispersion η_x along the DDX and NDX beamlines with the TDC off are shown in Fig. 2. The lattice functions and transverse spot size for the NDX are shown in Fig. 3.

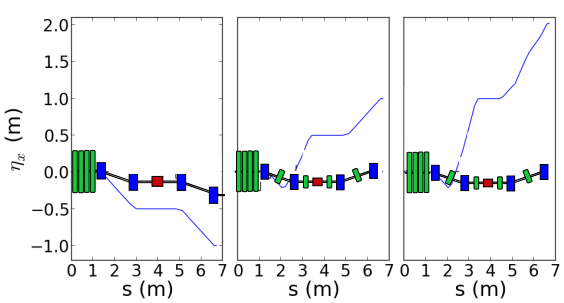

FIG. 2: Transverse dispersion η_x (blue) with the TDC off for the double-dogleg (left) and chicane with nominal-dispersion (middle) and boosted-dispersion (right) EEX designs, with the beamline schematic overlayed using the same coloring as Fig. 1.

Boosting the dispersion or placing greater demands on the longitudinal shaping makes controlling the beam size more difficult, which we discuss in the following sections. We also compared the DDX and NDX using simulations. For this study, we do not shape R_{51} and note that the "natural" R_{51} of each configuration is vastly different. This imposes additional constraints that may limit the quality of the emittance exchange.

Shaping the LPS entails controlling both R_{51} and R_{52} simulataneously. Generally, control of $R_{52} = 0$ is more vital to longitudinal shaping, as satisfying the condition allows for the overall spatial projection to transfer into

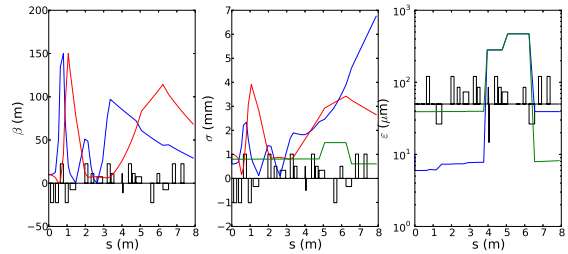

FIG. 3: Horizontal (blue), vertical (red), and longitudinal (green) lattice functions (left) RMS bunch sizes (middle), and normalized emittances (right), through the $\eta_x = 0.5$ m EEX with no shaping and initial emittances of 10 μm and an initial RMS bunch length of 0.8 m. The black rectangular outline shows the quadrupoles (thin) and dipole (wide) magnets.

the final current distribution, while R_{51} is adjusted to compress or lengthen the final distribution. To demonstrate the shaping, we cut the Gaussian transverse distribution in half along $x = 0$, then recenter the beam. We track the cut bunch through the EEX using various configurations and setting.

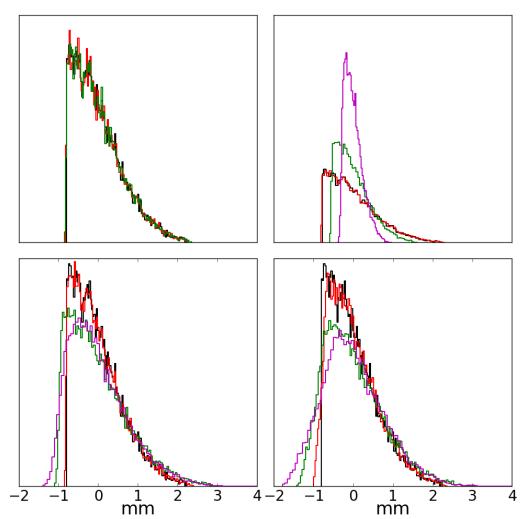

FIG. 4: Spatial projection of transverse and longitudinal phase spaces with x prior to the bunch compressor after being sheered in half with a mask (black) on each plot and the final longitudinal projection for various simnulation and shaping parameters. (top left) In ELEGANT with (green) and without (red) second order effects. (top right) In ELEGANT with R_{51} targetted 1.0 (red), 0.6 (green) and 0.2 (magenta). (lower left) In IMPACT-Z dispersion set to 0.5 m (red), 1.0 m (green) and 1.5 m (magenta), without space charge effects, and (lower right) the same simulations performed with 1.6 nC bunch charge with SC and CSR.

TABLE I: Emittance Exchange Values with IMPACT-Z

Des.	Q (nC)	η_x	R_{51}	R_{52}	$\mathcal{F}_{zx}$	$\mathcal{F}_{xz}$
DDX	0.0	0.5	-0.339	-0.259	1.33	1.00
DDX	1.6	0.5	-0.339	-0.259	5.51	1.65
NDX	0.0	0.5	1.00	-0.013	1.25	1.01
NDX	1.6	0.5	1.00	-0.013	4.24	1.67
BDX	0.0	1.0	1.17	-0.385	1.55	1.01
BDX	1.6	1.0	1.17	-0.385	5.09	1.63
BDX	0.0	1.5	1.04	-0.810	5.76	1.13
BDX	1.6	1.5	1.04	-0.810	8.85	1.50

III. CHICANE EEX WITH BOOSTED DISPERSION

Due to the reciprocal relationship between dispersion at the cavity strength and the required RF field of the TDC, "boosting" the dispersion of the beamlines reduces the requisite cavity power and cooling, technical limitations that decrease the feasibility of emittance exchangers particularly in HE beamlines. The four interior quadrupoles are used exclusively to tune the R_{16} of the doglegs, which colaterally adjusts the rest of the transfer matrix. This makes it more difficult to control the R_{51}, R_{52}, and betatron functions, placing soft-limits on how much the dispersion may be influenced, particularly when specific shaping is targetted. Increasing η_x at the TDC location by a factor of 2 or 3, decreases the field strength by a proportional factor, reducing the power and cooling requirements by an even greater factor.

Second-order effects are a constant detriment to emittance exchangers, and arise in TDCs, quadrupoles, and dipoles, reducing the quality of the exchange. Similarly, SC and CSR cause a degradation of the emittance exchange and intended longitudinal shaping. We model the EEX in the code IMPACT-Z, in which the SC interaction is modeled using a mean-field quasi-static particle-in-cell (PIC) algorithm. The code also includes a simple one-dimensional model for the CSR [12] that is produced in the dipole bends. Simulation parameters follow our studies in Ref. [6, 7].

Table I shows the qualities for many of the previous EEX setups and simulation parameters. The R_{51} and R_{52} values are the *achieved* values, rather than the target values; there is a distinction between the two due to the over-fitting that comes from constraining both betatron functions along the length of the full emittance exchanger at the same time as fixing the R_{51} and R_{52}. Collective effects distort the hard edge introduced by the transverse mask, while still transporting the overall shape of the bunch.

IV. APPLICATIONS AT ASTA

The implementation of an EEX beamline at ASTA will be staged. Currently, we foreseen to install an experiment to explore the performance of the NDX and BDX. This experiment will be located in the $\sim$ 50-MeV user area in the photoinjector. At a later stage we plan to implement the tested EEX at higher energy (most probably downstream of one cryomodule at 250 MeV). Such a beamline will be used to provide users with tunable emittance partion within the three degrees of freedom (when combined with the round-to-flat beam transform), or tailored current profile. This high-energy EEX may be used to tailor ramp current distributions for a possible dielectric energy doubler [13]. In the long-term, ASTA may also include a double emittance exchanger [5] and simulation studies are under way; an early design is shown in Fig. 5. Second-order effects in particular are a significant obstacle to operation of a double EEX.

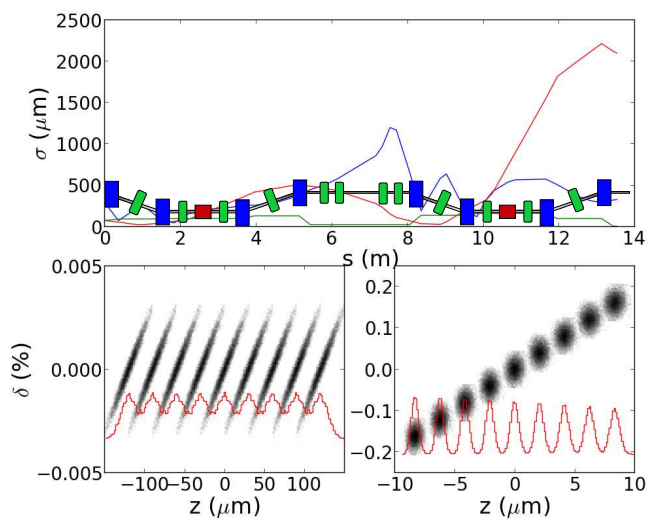

FIG. 5: Double emittance exchanger beamline (Top) with horizontal (blue), vertical (red) and longitudinal (green) RMS beam sizes, with schematic overlayed with same code as Fig. 1. LPS and projection (red) before first EEX (Lower Left) and after second EEX (Lower Right), using only first-order transfer matrices and no SC or CSR.

[1] P. Emma, et. al, PRSTAB 9, 100702 (2006).
[2] Y.-E. Sun, et. al, *Phys. Rev. Lett.* **105**, 234801 (2010).
[3] J. Ruan, et. al, *Phys. Rev. Lett.* **106**, 244801 (2011).
[4] P. Piot, FERMILAB-CONF-13-086-AD-APC (2013).
[5] A.A. Zholents, M.S. Zolotorev, ANL/APS/LS-327 (2011).
[6] C. R. Prokop, et. al, Fermilab Report No. FERMILAB-TM-2533-APC (2012).

[7] C. R. Prokop, et. al, *NIM A*, accepted (2013).
[8] M. Borland, APS LS-287, September 2000 (unpublished).
[9] Ji Qiang, et al., *Journ. Comp. Physics* **163**, p. 434 (2000).
[10] R.P. Fliller, unpublished, (2007).
[11] D. Edwards, *Fermilab TM*, (2007).
[12] E.L. Saldin, et. al, *NIM A* **A 398** p. 373-394 (1997).
[13] F. Lemery, et. al, these proceedings (2013).